MULTISCALE MODEL. SIMUL.
Vol. 7, No. 1, pp. 197–213

A MULTISCALE MODEL OF FIRST AND SECOND ORDER PHASE TRANSFORMATIONS WITH APPLICATION TO SMA SINGLE CRYSTALS*

VESSELIN STOILOV†

Abstract. This work aims to connect an atomistic model with continuum theory of phase transformations in shape memory alloys (SMAs). A formulation of the Helmholtz free energy potential based on Einstein potential has been developed. The atomic potential was used to describe the interatomic interactions in a biatomic crystal of NiTi. The microscopic expressions of the instantaneous mechanical (continuum) variables of mass, momentum, internal energy, and temperature have been derived in terms of the atomic variables. The developed Helmholtz thermodynamic potential is used in the context of the sharp phase front-based continuum framework proposed by Stoilov and Bhattacharyya [*Acta Mater.*, 50 (2002), pp. 4939–4952] to study the micro-macro transition during the thermomechanical response of NiTi crystals. The developed model has been successfully used to predict the response of a one-dimensional single crystal system.

Key words. multiscale model, Helmholtz free energy, shape memory alloys, NiTi

AMS subject classification. 82B26

DOI. 10.1137/070695940

1. Introduction. The ability to design materials with predetermined properties starting from their atomic structure has recently received significant attention. To design advanced materials from the bottom up not only requires full understanding of the individual building blocks (atom, molecules) but also deep knowledge of the simple construction units (clusters, grains etc.). These units span nano-meso-macro length scales, and bridging these scales is one of the main obstacles in the development of effective theoretical tools in the "bottom up" materials design.

There are two conceptually different approaches that have been taken to address multiscale modeling problems. The first approach involves the passing of critical information obtained from atomic-scale models to mesoscales. At the simplest level these could be elastic constants, thermal expansion coefficients, and other properties of materials that can be extracted from atomistic models and then used as constitutive material properties input for continuum models. For instance, information about dislocation slip systems and other dislocation properties have been used in the formulation of crystal plasticity models. More recently, atomistic or quantum level calculations of material separation have been performed [11, 8] to supply cohesive zone parameters for continuum models of fracture nucleation and propagation. The approach of "passing" information from smaller- to larger-scale models is rather powerful because no direct coupling of computational methods at different scales is needed. The applicability of such approaches is limited because the small-scale phenomena are generalized via studies of (usually) simple defect-free geometries that may not capture the full complexity of deformation and transformation that would emerge from a hypothetical, fully atomistic treatment.

*Received by the editors June 30, 2007; accepted for publication (in revised form) December 14, 2007; published electronically April 16, 2008.
http://www.siam.org/journals/mms/7-1/69594.html
†Department of Mechanical, Automotive and Materials Engineering, University of Windsor, Windsor N9B3P4, ON, Canada (vstoilov@uwindsor.ca).

The second major concept for multiscale modeling is the explicitly coupled models. These types of models retain the full atomistic detail in one or a few critical regions of the material, whereas the rest of the material is modeled by implementing a higher-scale approach. Explicitly coupled models are appropriate and useful when important atomic-scale phenomena are relatively localized in space, such as phase transformation fronts, crack propagation, grain boundaries, etc. In such multiscale models, atomistic phenomena are properly described where necessary while continuum mechanics approaches are used in surrounding regions. An example for such an approach is the macroscopic, atomistic, and ab initio dynamics (MAAD) method developed by Abraham, Broughton, and coworkers [5, 20]. In this method, three different computational methods, namely tight-binding (TB), molecular dynamics (MD), and finite element (FE), are concurrently linked together to simulate crack propagation in a brittle solid. TB is used to simulate the atomic bond breaking right at the crack-tip; MD is used to simulate the breaking at the region around the crack-tip; FEs are used in the region far from the crack-tip where the deformation field is generally smooth. The dynamics of the entire system is governed by a total Hamiltonian function that combines the separate Hamiltonians of the three different regions. While MAAD has been successfully applied to brittle fracture in Si, some major issues still remain. The most significant of these issues lies in the coupling of the different levels of simulations. In MAAD, the coupling is accomplished by assuming that each simulation contributes an equal amount of energy to the total energy in the transition region. However, no rigorous studies have been performed to quantify the effectiveness of this method in eliminating spurious wave reflection at the simulation boundaries. Another concurrent method developed recently is the quasi-continuum (QC) method [3, 4, 25, 22, 17]. In this method, the continuum framework and continuum particle concept are retained, while the macroscopic constitutive law is replaced by that from direct atomistic simulations. Each continuum particle is regarded as a small crystallite surrounding a representative atom. The strain energy associated with the representative atom can be computed by summing up the interatomic potential of the crystallite following the Cauchy–Born rule. In overcoming the requirement of grading FE mesh down to the lattice size, as in the QC and MAAD methods, a concurrent coupling method, called the "bridging scale method," has been recently developed by Liu and coworkers [7, 19, 26]. A unique characteristic of this method is that it is assumed that the FE and MD solutions exist simultaneously in the entire computational domain and MD calculations are performed only in the regions that are necessary.

In this paper we shall focus on the development of a multiscale model of first and second order phase transformations. In the second half of the paper the model is used to study the phase transformations in shape memory alloys (SMAs). The phase transformation in SMAs is a first order transition, accompanied by the release or absorption of energy when the phase changes occur. The proposed multiscale model consists of two models: meso- and nanoscale models. These models are linked through the quantum mechanics definition of the Helmholtz free energy function [15]. The mesoscale model is based on the theoretical framework suggested by Stoilov and Bhattacharyya [23]. This model accommodates any formulation of the Helmholtz free energy function and renders a complete solution to the continuum phase transformation problem. The continuum description of the phase changes in SMAs includes balance laws (of mass, linear momentum, and energy), the material's constitutive equations, and the constitutive equation at the phase boundary [23, 24]. The nanoscale model is based on the calculation of the total potential energy of interaction between the atoms/molecules of the system. This involves an explicit definition of in-

teratomic potential. In this study an example of the implementation of Einstein-type potential is used to account for the nanolevel phase transformation in a NiTi alloy.

The paper is organized into seven sections. Section 2 outlines the essence of the adopted multiscale approach, section 3 discusses the general formulation of the Helmholtz free energy in terms of interatomic potentials, section 4 gives a brief description of the continuum (mesoscale) model, and section 5 discusses the implementation of the Einstein potential to predict the phase transformation NiTi single nanocrystal. Section 6 is devoted to the numerical results of the proposed approach, and all findings are summarized in section 7.

2. Bridging the scales-model formulation. In the "macroscopic world," we study the bulk properties of matter, which means that we study samples containing on the order of 10^{23} atoms/molecules. The main theoretical framework for the study of bulk properties is thermodynamics and continuum mechanics. On the other hand, we also study the "microscopic world," where we are concerned with the properties of individual atoms/molecules. The usual theoretical framework of the microscopic world is quantum mechanics (or sometimes classical mechanics), and the fundamental equations are Schrödinger equations. However, the properties of bulk matter are predetermined by the properties of the particles of which it is composed. So in order to bridge the different scales, an explicit relationship between the atomic presentation and the constitutive law for the material should be found. The constitutive law of a material can be represented as one of the four thermodynamics potentials: internal energy, Helmhotz free energy, Gibbs free energy, and the enthalpy. For the purposes of the model developed in this study, the constitutive laws of the materials are represented by the Helmholtz free energy. From the atomistic point of view, the Helmholtz free energy is explicitly defined by the atomic structure and its total energy through the statistical partition function. On the other hand, the Helmholtz free energy uniquely defines almost all macroscopic (mesoscale) thermomechanical constitutive laws (stress-strain, entropy-temperature, etc.) governing the material's behavior (see Figure 2.1). Thus, the Helmholtz free energy serves as a natural bridge between the atomistic and macroscopic phenomena, and it will be utilized in the proposed multiscale model.

The atomistic definition of the Helmholtz free energy is related to the partition function for a canonical ensemble, Z, as

$$\Psi = -k\theta \ln Z, \tag{2.1}$$

where Ψ denotes the Helmholtz free energy, k is the Boltzmann constant, and θ is the absolute temperature. The quantum mechanical presentation of the partition function Z (for a canonical ensemble) is [18]

$$Z = \sum_{E_r} g(E_r) e^{-\frac{E_r}{k\theta}}, \tag{2.2}$$

where $g(E_r)$ is the number of particles possessing E_r energy.

Equations (2.1) and (2.2) are remarkable in that the partition function depends on atomic/molecular properties through the quantum mechanical energies E_j, whereas the left-hand side of (2.1) is a macroscopic, classical thermodynamic quantity. Therefore, these equations allow thermodynamic properties to be interpreted and calculated in terms of atomic/molecular properties.

In classical mechanics of continuum the system does not have discrete energy levels. The energy, like the other variables characterizing the state of the system, is

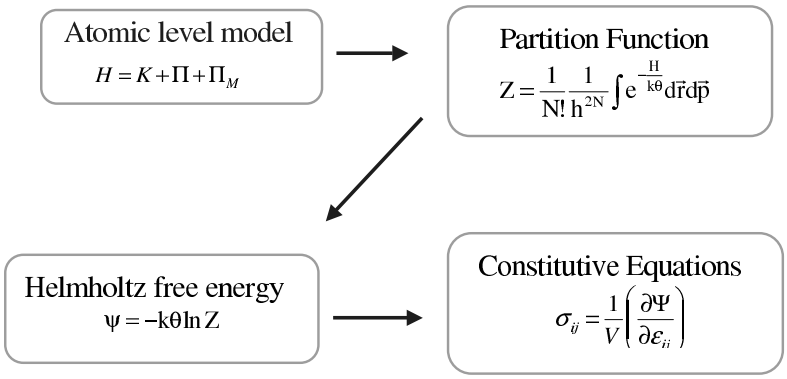

FIG. 2.1. *Schematic of the multiscale approach.*

a continuous variable. In quasi-classical form, for the atomic system the partition function is [18]

$$Z = \frac{1}{N!}\frac{1}{h^{3N}}\int e^{-\frac{\mathcal{H}}{k\theta}} d\mathbf{r} d\mathbf{p}, \tag{2.3}$$

where $\mathbf{r}$, $\mathbf{p}$ are the coordinates and momenta of the particles in $[\mathbf{r}, \mathbf{r}+d\mathbf{r}] \cup [\mathbf{p}, \mathbf{p}+d\mathbf{p}]$, h is the Planck constant, and $\mathcal{H}$ is the Hamiltonian of the system. The Hamiltonian can be presented as a sum of the kinetic and the potential energy of the system

$$\mathcal{H} = \mathcal{K} + \mathcal{P}. \tag{2.4}$$

Since the kinetic energy is only momenta dependent, whereas the potential energy function is position dependent, the partition function factorizes into a product of kinetic (ideal gas) and potential (excess) parts:

$$Z = \frac{1}{N!}\frac{1}{h^{3N}}\left(\int e^{-\frac{\mathcal{K}}{k\theta}} d\mathbf{p}\right)\left(\int e^{-\frac{\mathcal{P}}{k\theta}} d\mathbf{r}\right) = Z^{id} Z^{ex}. \tag{2.5}$$

For a system of atoms with mass, m, the kinetic part has a standard (as ideal gas) presentation

$$Z^{id} = \frac{V^N}{N! \Lambda^{3N}}, \tag{2.6}$$

where Λ is the thermal de Broglie wavelength

$$\Lambda = \left(\frac{h^2}{2\pi m k\theta}\right)^{\frac{1}{2}}. \tag{2.7}$$

The excess part of the partition function reads

$$Z^{ex} = \frac{1}{V^N}\left(\int e^{-\frac{\mathcal{P}}{k\theta}} d\mathbf{r}\right), \tag{2.8}$$

where V is the volume of the system. By combining (2.1) with (2.5)–(2.8), an explicit form of the Helmholtz energy can be derived if the interaction potential, $\mathcal{P}(\mathbf{r})$, is known.

3. Helmholtz free energy function based on interatomic potential.

3.1. Thermodynamics of the one-dimensional system. We shall consider an equilibrium isothermal system of N particles possessing only one degree of freedom each and distributed on a segment of axis Ox of length L. The partition function for such a system is given by

$$Z = Z^{id} Z^{ex} = \frac{V^N}{N!} \left(\frac{2\pi mk\theta}{h^2} \right)^{\frac{N}{2}} Z^{ex}. \tag{3.1}$$

The constitutive law for the specified material can be derived using one of the Maxwell relationships [15] along with (2.1):

$$\sigma = \frac{1}{V} \left(\frac{\partial \Psi}{\partial \epsilon} \right)_\theta = -\frac{k\theta}{V} \frac{\partial \ln Z^{ex}}{\partial \epsilon}, \tag{3.2}$$

where we used the notation $\left(\frac{\partial \zeta}{\partial \chi}\right)_\kappa$ to denote a partial derivative at constant variable κ. Furthermore we assume that the total interactions in the system are composed of the interactions of individual pairs of particles described by the potential u_i. If we then assume in addition that the potential u_i is a short range in which each particle interacts only with the two closest neighbors (one from each side), we obtain

$$\mathcal{P} = \sum_{1 \le i \le N-1} u_i(x_{i+1} - x_i). \tag{3.3}$$

For the derivation of the following relation a formalism similar to the one developed by Gursey (see Fisher [6]) is used (see Appendix A). When N is a large number, the asymptotic form of the excess partition function follows from [6] as

$$Z^{ex} = \frac{N!}{V^N} e^{-\frac{\sigma \epsilon V}{k\theta}} \left(\phi(\sigma, \theta)\right)^{N+1}, \tag{3.4}$$

where

$$\phi(\sigma, \theta) = \int_0^\infty e^{\left(-\frac{u_i(x) + \sigma A x}{k\theta}\right)} dx, \tag{3.5}$$

where A is the cross-sectional area of the one-dimensional system. Using (2.1), (3.4), and (3.1), the Helmholtz free energy per unit volume, ψ ($\psi = \frac{\Psi}{V}$), is obtained:

$$\begin{aligned} \psi = \sigma\epsilon &- \frac{1}{2V} Nk\theta \ln \left(\frac{2\pi mk\theta}{h^2} \right) \\ &- \frac{(N+1)}{V} k\theta \ln(\phi(\sigma, \theta)). \end{aligned} \tag{3.6}$$

Each of the terms in (3.6) can be attributed to different types of energy. The first term represents the mechanical energy of the system, whereas the second and the third terms are the chemical and thermomechanical contributions to the total energy. In the next section we illustrate the application of the developed theory to the one-dimensional phase transformation problem in SMAs.

4. Mesoscale model of the phase transformation in single crystal SMAs. In this section we shall focus on theoretical framework for the phase transformations in a spatially one-dimensional SMA system. For complete derivation of the theoretical framework we refer the reader to Stoilov and Bhattacharyya [23]. In this section will briefly outline the basics of the approach.

4.1. Constitutive equations. We consider a class of materials for which the stress, σ, the specific entropy, η, and the specific internal energy, u, are dependent on the Lagrangian strain, ϵ, and the temperature, θ, while the heat flux, q, is given by the Fourier law of heat conduction. These relations are respectively stated as

$$\sigma \equiv \sigma(\epsilon, \theta), \quad \eta \equiv \eta(\epsilon, \theta), \quad u \equiv u(\epsilon, \theta),$$
$$q = -K_T \frac{\partial \theta}{\partial X}, \tag{4.1}$$

where the Lagrangian strain follows from the deformation gradient, F, as

$$\epsilon = \frac{1}{2}\left(F^2 - 1\right), \tag{4.2}$$

and the parameter, K_T, in (4.1) is the thermal conductivity. In particular, the stress σ, entropy η, and internal energy u may be derived from the Helmholtz free energy function, $\psi \equiv \psi(\epsilon, \theta)$ (see (3.6)), as [15]

$$\sigma = \left(\frac{\partial \psi}{\partial \epsilon}\right)_\theta, \qquad \eta = -\left(\frac{\partial \psi}{\partial \theta}\right)_\epsilon, \qquad u = \psi + \theta\eta. \tag{4.3}$$

For two phases to coexist in thermodynamic equilibrium, the stress (σ), the temperature (θ), and the chemical potential (μ) have to be continuous at their interface [15]. For irreversible processes not too far away from thermodynamic equilibrium, the latter two quantities remain continuous at the phase boundary, or equivalently, their jumps vanish. Thus

$$[\theta] = 0, \qquad [\mu(\sigma, \theta)] = 0 \qquad \text{at} \qquad x = x_s(t). \tag{4.4}$$

Denoting $\theta(x_s(t)) = \theta_s$,

$$\left[\epsilon \frac{\partial \sigma}{\partial \theta_s}\right] = -[\eta] \qquad \text{at} \qquad x = x_s(t), \tag{4.5}$$

(4.5) is the generalized Clausius–Clapeyron equation [23].

4.2. Conservation laws. In the absence of body forces, the conservation of linear momentum away from the phase boundary ($x = x_s(t)$) is given by

$$\frac{\partial \sigma}{\partial X} = \rho_0 \frac{dV}{dt} \qquad \text{at} \qquad x \neq x_s(t), \tag{4.6}$$

where the coordinate, X, is the location of a particle in the reference configuration, t is time, $\sigma \equiv \sigma(X, t)$ is the uniaxial first Piola–Kirchhoff stress (also referred to sometimes as the "nominal stress"), $\rho_0 \equiv \rho_0(X)$ is the mass density in the reference configuration, and V is the particle velocity. The conservation of energy is

$$\frac{\partial q}{\partial X} + \sigma \frac{dF}{dt} + \rho_0 r = \frac{du}{dt} \qquad \text{at} \qquad x \neq x_s(t), \tag{4.7}$$

where q is the heat flux, F is the deformation gradient (defined below), $r \equiv r(X, t)$ is the heat source per unit mass, and u is the internal energy per unit volume of the reference configuration. In particular, we define

$$F = 1 + \frac{\partial w}{\partial X}, \quad \text{where} \quad w = x - X, \tag{4.8}$$

w being the displacement of a particle from its reference configuration. The conservation of mass is stated as

$$\frac{d\rho}{dt} + \rho\frac{\partial V}{\partial x} = 0 \qquad \text{at} \qquad x \neq x_s(t), \tag{4.9}$$

where ρ is the mass density in the deformed configuration. Denoting a jump in a quantity, $\mathcal{A}$, at the phase boundary as $[\mathcal{A}]$ and defining it as $[\mathcal{A}] = \lim_{\triangle\to 0}\mathcal{A}(x_s+\triangle,t) - \lim_{\triangle\to 0}\mathcal{A}(x_s-\triangle,t)$, where $\Delta > 0$, the conservation of linear momentum, energy, and mass at the phase boundary ($x = x_s(t)$), respectively, imply the following jumps:

$$\begin{aligned} [\sigma] = -\rho_0[V]V_s, \quad [q] = -\left[u + \frac{1}{2}\rho_0 V^2\right]V_s - [V\sigma], \\ [V] = -V_s[F], \end{aligned} \tag{4.10}$$

where $V_s = \partial x_s/\partial t$ is the phase boundary velocity.

5. One-dimensional phase transformation in a NiTi nanocrystal. In this section we apply the theory outlined in the previous section to describe the phase transformation in a NiTi single crystal. The considered crystal is one-dimensional, and both phases, austenite and martensite, are represented as one-dimensional arrays of atoms, as shown in Figure 5.1. The two arrays have different lattice constants and different energies of interactions. The different lattice constants will determine the magnitude of the transformation strain, and the different interaction energies will represent the release/absorption of heat during the phase transformation process. The interatomic potential adopted here is an Einstein-type potential [18] defined as

$$u_i(x) = \begin{cases} \frac{\gamma}{2}\left(x_{i+1} - x_i - a_0\right)^2 & \text{for} \quad |x_{i+1} - x_i| \leq a_0, \\ \infty & \text{otherwise}, \end{cases} \tag{5.1}$$

where a_0 is the lattice constant, γ is the stiffness of the bond, and x ($x = x_{i+1} - x_i$) is the instantaneous value of the bond length. This potential defines the interatomic interactions as linear elastic, which is a reasonable approximation for most solid materials, assuming small atomic displacements from the equilibrium positions [18].

5.1. Thermodynamics of the phase transformation. In order to treat a system by statistical mechanics, one must calculate the configuration or excess partition function Z^{ex}. We shall assume that the potential energy U of the system results from interatomic/molecular potentials between the atoms. For the one-dimensional system with cross-section, A, the excess part of the partition function follows from (3.4). The complete derivation of (5.2) is included in Appendix A:

$$Z^{ex} = \frac{1}{V^N}\, e^{-\frac{\sigma A L_0(1+\epsilon)}{k\theta}} \left[\phi(\sigma,\theta)\right]^{N+1}. \tag{5.2}$$

After substituting (5.1) into (3.5) one can obtain the explicit form of ϕ,

$$\phi(\sigma,\theta) = \frac{a_0}{2}\sqrt{\frac{\pi}{\beta}} e^{\frac{\sigma^2 A^2 a_0^2}{4k^2\theta^2\beta}} \left(\operatorname{erf}\left(\frac{-2\beta k\theta + \sigma A a_0}{2k\theta\sqrt{\beta}}\right) - \operatorname{erf}\left(\frac{\sigma A a_0}{2k\theta\sqrt{\beta}}\right)\right), \tag{5.3}$$

where β is the ratio of the energy of the bond to the thermal energy

$$\beta = \frac{\gamma a_0^2}{2k\theta}. \tag{5.4}$$

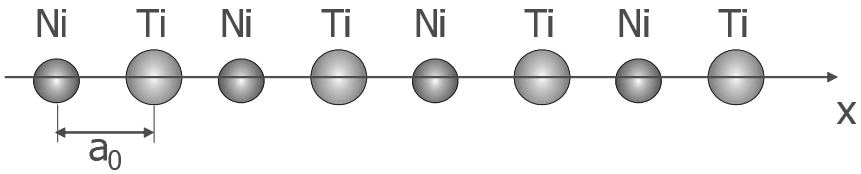

FIG. 5.1. *Schematic of the one-dimensional NiTi single crystal.*

Since ϕ is in terms of σ and θ, it is more convenient to use the Gibbs free energy instead of the first equation in (4.1) to obtain the equation of state (Hooke's law):

$$G = \psi - \sigma\epsilon = -\frac{1}{2V} N k\theta \ln\left(\frac{2\pi m k\theta}{h^2}\right) - \frac{(N+1)}{V} k\theta \ln(\phi(\sigma,\theta)). \tag{5.5}$$

From the definition of the Gibbs free energy (see (5.5)) the equation of state follows as

$$\epsilon = -\left(\frac{\partial G}{\partial \sigma}\right)_\theta = \frac{(N+1)}{V} k\theta \frac{1}{\phi(\sigma,\theta)} \left(\frac{\partial \phi}{\partial \sigma}\right)_\theta. \tag{5.6}$$

Equation (5.6) combined with (5.3) can be expanded into series with respect to stress, σ. Keeping only linear terms the strain can be obtained as

$$\epsilon = -\frac{(N+1)a_0 A\left(e^{-\beta}-1\right)}{\operatorname{erf}\left(\sqrt{\beta}\right) V\sqrt{\pi\beta}} \tag{5.7}$$
$$-\frac{1}{2}\frac{(N+1)a_0^2 A^2\left(-\pi\ \operatorname{erf}(\sqrt{\beta})^2 + 2\sqrt{\pi\beta}\ \operatorname{erf}(\sqrt{\beta})\, e^{-\beta} + 2e^{-2\beta} - 4e^{-\beta} + 2\right)}{\pi V \beta k\theta\ \operatorname{erf}(\sqrt{\beta})^2}\sigma.$$

In solids, the energy of the interatomic bonds significantly exceeds the energy of thermal motion; therefore parameter β will have a value well above 1 ($\beta \gg 1$). For large β, (5.7) becomes

$$\epsilon = \frac{(N+1)a_0 A}{V\sqrt{\pi\beta}} + \frac{(N+1)a_0^2 A^2(\pi-2)}{2\pi V\beta k\theta}\sigma. \tag{5.8}$$

If the Young modulus, E, and the coefficient of thermal expansion, α, are defined as

$$E = \frac{\pi\gamma a_0^2}{V_c(\pi-2)}, \qquad \alpha = \sqrt{\frac{k}{2\pi\gamma a_0^2\theta_0}}, \tag{5.9}$$

the strain in the system will be given by

$$\epsilon = \alpha(\theta-\theta_0) + \frac{\sigma}{E} + \epsilon_T, \tag{5.10}$$

where ϵ_T is prestrain (reference strain) at $\theta = \theta_0$ and $\sigma = 0$. The thermal expansion coefficient, α, was obtained from the first term of (5.8) for small temperature deviation from a reference temperature, θ_0:

$$\zeta(\theta) = \frac{(N+1)a_0 A}{V\sqrt{\pi\beta}} \approx \frac{1}{\sqrt{\pi\beta}} = \sqrt{\frac{2k\theta}{\pi\gamma a_0^2}} \tag{5.11}$$
$$\approx \sqrt{\frac{2k\theta_0}{\pi\gamma a_0^2}} + \sqrt{\frac{k}{2\pi\gamma a_0^2\theta_0}}(\theta-\theta_0) = \epsilon_T + \alpha(\theta-\theta_0).$$

In the derivation of the Young modulus, E, the coefficient of thermal expansion, α (see (5.9)), and (5.11) we used the definition of lattice cell volume, V_c:

$$V_c = a_0 A \approx \frac{V}{N+1}.$$

Next we formulate the heat capacity in terms of entropy:

$$C_\epsilon = \theta \left(\frac{\partial \eta}{\partial \theta}\right)_\epsilon. \tag{5.12}$$

The Helmholtz free energy per unit volume, ψ, is obtained from the first two equations in (4.3) and

$$d\psi = \left(\frac{\partial \psi}{\partial \epsilon}\right)_\theta d\epsilon + \left(\frac{\partial \psi}{\partial \theta}\right)_\epsilon d\theta, \tag{5.13}$$

which yields the following definition of ψ:

$$d\psi = \sigma d\epsilon - \eta d\theta. \tag{5.14}$$

By combining (5.14), (5.10), and (5.12) and integrating consecutively over the stain, ϵ, and the temperature, θ, the Helmholtz free energy becomes

$$\begin{aligned}\psi = {} & \frac{1}{2} E \left(\epsilon - \epsilon_T\right)^2 - E\alpha \left(\epsilon - \epsilon_T\right)\left(\theta - \theta_0\right) \\ & + C_\epsilon \theta \left(1 - \ln \frac{\theta}{\theta_0}\right) + \psi_0.\end{aligned} \tag{5.15}$$

The expressions for entropy, internal energy, and heat capacity follow from (4.1) and (3.6) as

$$\begin{aligned}\eta = {} & \frac{1}{2V} Nk \left(1 + \ln\left(\frac{2\pi m k \theta}{h^2}\right)\right) + \frac{(N+1)}{V} k \ln(\phi(\sigma,\theta)) \\ & + \frac{(N+1)}{V} k\theta \frac{1}{\phi(\sigma,\theta)} \left(\frac{\partial \phi(\sigma,\theta)}{\partial \theta}\right)_\sigma,\end{aligned} \tag{5.16}$$

$$u = \sigma\epsilon + \frac{1}{2V} Nk\theta + \frac{(N+1)}{V} k\theta \frac{1}{\phi(\sigma,\theta)} \left(\frac{\partial \phi(\sigma,\theta)}{\partial \theta}\right)_\sigma, \tag{5.17}$$

$$\begin{aligned}C_\epsilon = {} & \frac{1}{2V} Nk + \frac{2(N+1)}{V} k\theta \frac{1}{\phi(\sigma,\theta)} \left(\frac{\partial \phi(\sigma,\theta)}{\partial \theta}\right)_\sigma \\ & - \frac{(N+1)}{V} k\theta^2 \frac{1}{\phi^2(\sigma,\theta)} \left(\frac{\partial \phi(\sigma,\theta)}{\partial \theta}\right)_\sigma^2 + \frac{(N+1)}{V} k\theta^2 \frac{1}{\phi(\sigma,\theta)} \left(\frac{\partial^2 \phi(\sigma,\theta)}{\partial \theta^2}\right)_\sigma.\end{aligned} \tag{5.18}$$

The final equation, needed to complete the description of the system, is the generalized Clausius–Clapeyron equation. The jump of the entropy at the phase boundary can be derived from (5.16):

$$\begin{aligned}[\eta] = {} & \left[\frac{1}{2V} Nk \ln\left(\frac{2\pi m k \theta}{h^2}\right) + \frac{(N+1)}{V} k \ln(\phi(\sigma,\theta))\right. \\ & \left. + \frac{(N+1)}{V} k\theta \frac{1}{\phi(\sigma,\theta)} \left(\frac{\partial \phi(\sigma,\theta)}{\partial \theta}\right)_\sigma\right].\end{aligned} \tag{5.19}$$

The right-hand side of (4.5) contains an explicit derivative of the stress with respect to the temperature. Since the stress has been defined implicitly (see (5.6)) it is computed using the implicit differentiation rule:

$$\left(\frac{\partial\sigma}{\partial\theta}\right)_{\epsilon} = -\frac{\left(\frac{\partial\epsilon}{\partial\theta}\right)_{\sigma}}{\left(\frac{\partial\epsilon}{\partial\sigma}\right)_{\theta}}, \tag{5.20}$$

$$\begin{aligned}&\left[\frac{\epsilon}{\theta}\frac{\frac{\phi}{\theta}\left(\frac{\partial\phi}{\partial\sigma}\right)_{\theta} - \left(\frac{\partial\phi}{\partial\sigma}\right)_{\theta}\left(\frac{\partial\phi}{\partial\theta}\right)_{\sigma} + \phi\left(\frac{\partial^2\phi}{\partial\sigma\partial\theta}\right)}{\left(\frac{\partial\phi}{\partial\sigma}\right)_{\theta}^2 + \phi\left(\frac{\partial^2\phi}{\partial\sigma^2}\right)_{\theta}}\right] \\ &= \left[\frac{1}{2V}Nk\ln\left(\frac{2\pi mk\theta}{h^2}\right) + \frac{(N+1)}{V}k\ln(\phi(\sigma,\theta))\right. \\ &\qquad \left. + \frac{(N+1)}{V}k\theta\frac{1}{\phi(\sigma,\theta)}\left(\frac{\partial\phi(\sigma,\theta)}{\partial\theta}\right)_{\sigma}\right].\end{aligned} \tag{5.21}$$

The last equation completes the system of equations ((4.6)–(4.10), (5.15), and (5.21)) derived for the SMA material, in terms of the function ϕ. The addition of the definition of ϕ (see (3.5)) renders a unique solution of the mathematical problem. The numerical method for the solution of the system of equations is described in Stoilov and Bhattacharyya [23]. The additional function $\phi(\sigma,\theta)$ was tabulated for the range of the stress and temperatures and was used as an input. All necessary derivatives of $\phi(\sigma,\theta)$ were computed numerically.

6. Results and discussion. The theoretical values of the Young modulus, E, and the thermal expansion coefficient, α, were obtained using (5.9). The stiffness constant, γ, in the adopted atomic potential was estimated by assuming that an atom would have enough energy to leave the system if it could be displaced by a distance equivalent to one lattice constant, a_0. Thus the energy of evaporation, E_v, per single atom can be expressed as

$$E_v = \frac{1}{2}\gamma a_0^2. \tag{6.1}$$

With (6.1), the Young modulus, E, and the thermal expansion coefficient, α, can be determined by using that

$$E = \frac{2\pi E_v}{V_c(\pi-2)}, \qquad \alpha = \sqrt{\frac{k}{4\pi E_v\theta_0}}. \tag{6.2}$$

6.1. Experimental verification. A comparison between the computed values of the Young modulus, E, the thermal expansion coefficient, α, and the corresponding experimental data, for the number of metals with body center cubic (bcc), hexagonal close-packed (hcp), and cubic close-packed (ccp) lattice structures, is shown in Figures 6.1 and 6.2. The theoretically predicted values are in good agreement with the experiment for most of the metals. However, some deviation is observed for metals with mainly ccp lattice structure such as Ir, Rh, etc. In these cases the theoretical prediction significantly underestimates the experimental values, which is probably due to the fact that in the ccp the second, third, etc., nearest neighbors make a significant contribution to the total energy of an atom, which is not taken into account by the adopted interatomic potential.

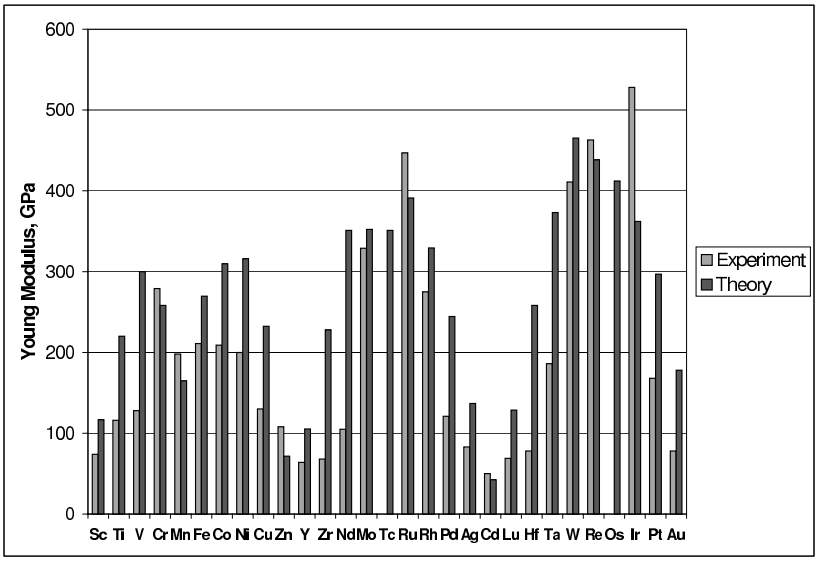

FIG. 6.1. *Young modulus for metals. Comparison with experiment* [10, 12].

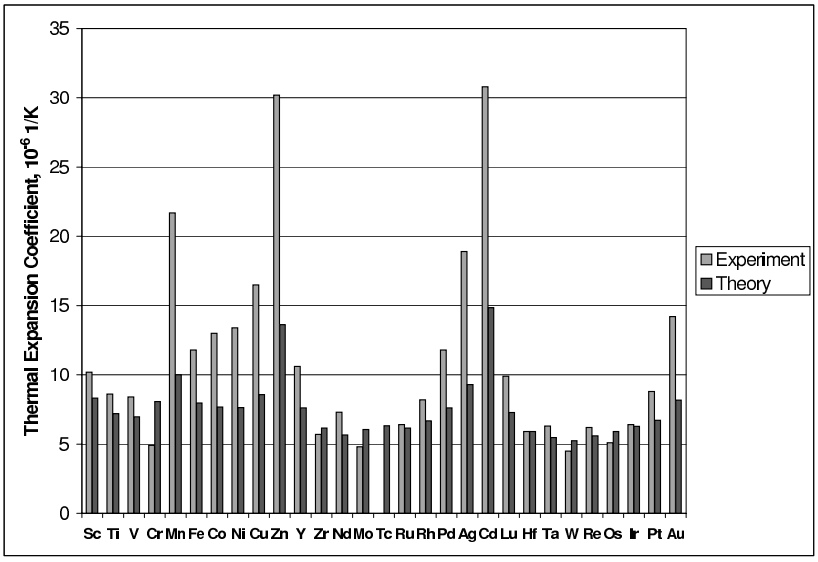

FIG. 6.2. *Thermal expansion coefficient. Comparison with experimental data* [16].

6.1.1. Heat capacity. The heat capacity deserves special attention. A good test for the result is the value of the obtained heat capacity at high temperatures. In the limit of high temperature ($T \to \infty$), C_v reaches a limit value of $C_v = \frac{3}{2}k$ (see (5.18) and (5.3)), which is the heat capacity of ideal gas per unit particle. This limit value of C_v corresponds to 50% deviation from the Debye predictions of $C_v = 3k$ for solids. The observed discrepancy could be explained with not taking into account the contribution of the vibration energy to the kinetic energy of the system.

6.2. Phase transformation in NiTi. As mentioned earlier the studies presented here are primarily focused on the development of a multiscale model of the

TABLE 6.1
List of material and geometric input parameters for Ti-50.1%atNi.

Parameter	Symbol	NiTi single crystal	
		Value	Ref.
No. of atoms	N_A	2500	-
Lattice constants	a_A	3.01Å	[14]
	a_M	3.19Å	-
Length	L	$752.5nm$	-
Perimeter of the cross-section	P	$0.157\mu m$	-
Area of the cross-section	A	$7.85 \times 10^{-15} m^2$	-
Mass density	ρ_0	$6450kg/m^3$	[13]
Uniaxial phase transformation strain	ε_{ph}	0.06	[1]
Latent heat of phase transformation	λ_{ph}	$0.121GJ/m^3$	[1]
Thermal conductivity	$k_{Austenite}$	$14W/(mK)$	[1]
	$k_{Martensite}$	$28W/(mK)$	[1]
Convective coefficients	h_L	$77W/(m^2K)$	[1]
	h_b	0	-

phase transformations in SMAs. In this section, we use the developed theory to predict the stress-induced phase transformation at constant deformation rate in a NiTi single crystal under uniaxial loading. The NiTi single nanocrystal was represented as a one-dimensional array of alternating Ni and Ti atoms. The lattice constant of the austenitic and martensitic phases were selected to be $a_A = 3.01$ Å [14] (see Table 6.1) and $a_M = (1 + \epsilon_{ph})a_A$, respectively. A list of the used material parameters and their values are presented in Table 6.1. Since the deformation gradient in most SMAs is small $\left(\frac{\partial w}{\partial x} \ll 1\right)$ away from the phase boundary, the "small strain" approximation for the following sample calculations will be invoked:

$$\epsilon \approx 1 - F = 1 - \frac{\Delta l}{l}. \tag{6.3}$$

The computed macroscopic pseudoelastic curves for three different ambient temperatures are shown in Figures 6.3–6.5. The model predictions are consistent with the experimental observations of Hamilton et al. [21] on single crystal $Ti - 50.1\%atNi$. Hamilton et al. [21] observed an increase in the values of the magnitude of the stress necessary to initiate the austenite-to-martensite phase transformation with the increase of the ambient temperature. This is also in agreement with the computations here. There are, however, some discrepancies. First, the predicted constant stress response during unloading deviates from the experimentally observed stress trend of decrease. Second, the experimental values of the magnitude of the stress necessary to initiate the reverse martensite-to-austenite phase transformation are higher than the model predictions. This in turn initiates a phase transformation at higher stress and reaches unrecoverable strains of an order of 0.2%. A possible explanation for these discrepancies could be the much smaller heat capacity predicted by the atomistic model (see section 6.1.1). In the simulations, the two times smaller heat capacity makes characteristic time response, t_{ch}, to the latent heat flux, two times smaller ($\Delta\theta \sim e^{-\frac{t}{t_{ch}}}$, $t_{ch} = \frac{\rho C_v V}{h A_s}$ [9]). Therefore, the predicted phase transformation during both, loading and unloading parts of the cycle, is virtually isothermal, which is shown as constant stresses during the transformation simulations. In contrast, the experiment showed that the loading and unloading parts of the cycle have different natures. While the slow loading is close to isothermal conditions and practically coincides with the simulation predictions, the quick unloading takes much less time than the real

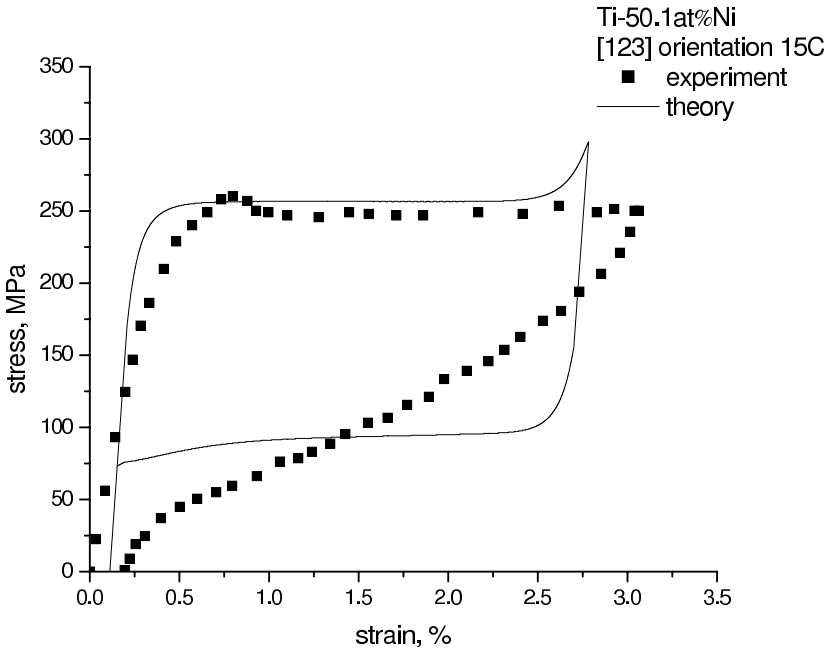

FIG. 6.3. *Experimental and theoretical stress-strain curves for single crystal Ti-50.1at%Ni* [123] *orientation* $\theta_{amb} = 15C$ [21].

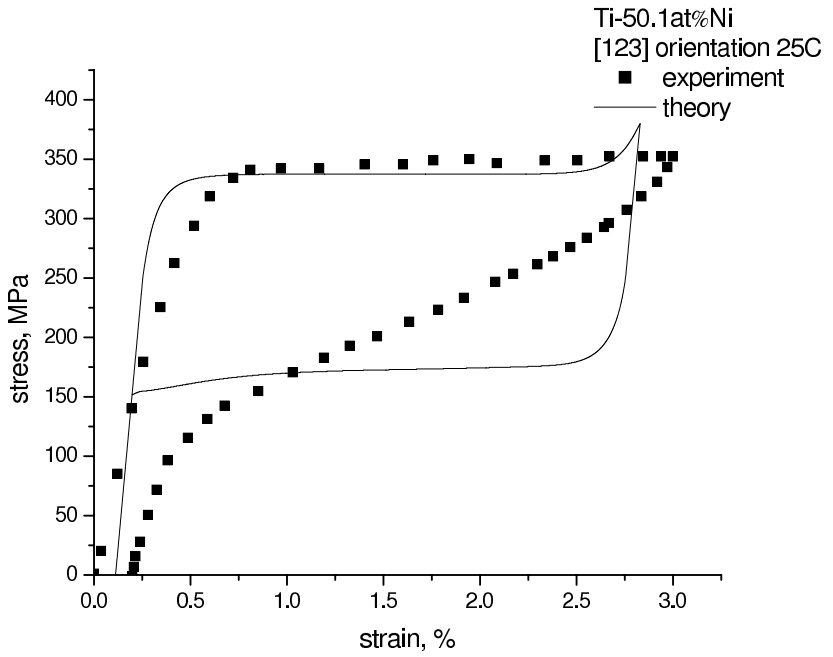

FIG. 6.4. *Experimental and theoretical stress-strain curves for single crystal Ti-50.1at%Ni* [123] *orientation* $\theta_{amb} = 25C$ [21].

characteristic response time, t_{ch}, and thus significantly deviates from the virtually isothermal predictions of the model.

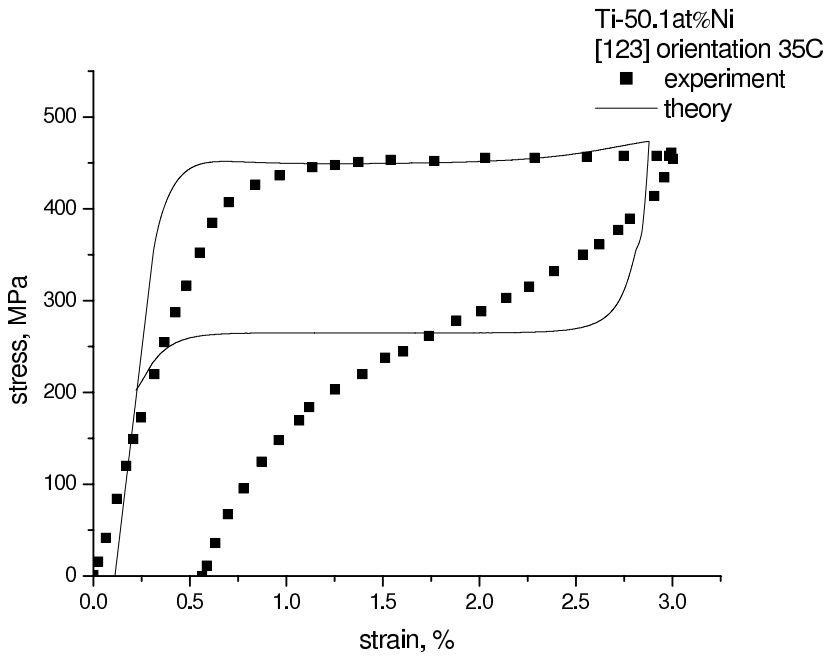

FIG. 6.5. *Experimental and theoretical stress-strain curves for single crystal Ti-50.1at%Ni* [123] *orientation* $\theta_{amb} = 35C$ [21].

7. Conclusions. We have developed a multiscale model of phase transformation for SMAs. Apart from the continuum formulation [23] we have proposed an atomic level model which was coupled with the continuum model through the quantum mechanics definition of the Helmholtz free energy function. It is also demonstrated that the proposed approach successfully models the one-dimensional phase transformation in NiTi single crystal. In addition the authors believe that implementation of vibration degrees of freedom and a better interatomic potentials such as Sutton–Chen or the modified embedded atom method [2] potentials are to improve the model performance.

Appendix A. Excess partition function. We shall assume that the potential energy U of the system results from interatomic/molecular potentials between the atoms. If we denote the potential energy between atoms i and j, when the distance $r_{ij} = |\mathbf{r}_i - \mathbf{r}_j|$ apart, by $u_{ij} \equiv u(r_{ij})$, then we write the potential energy of an ensemble of N atoms as

$$\mathcal{P} = \sum_{i=1}^{N} \sum_{j=i+1}^{N} u_{ij}. \tag{A.1}$$

After substituting (A.1) into (2.8) the excess part of the partition function becomes

$$Z_{ex} = \frac{1}{V^N} \int d^3\mathbf{r}_1 \dots d^3\mathbf{r}_N \prod e^{-\frac{u_{ij}}{k\theta}}, \tag{A.2}$$

where the product is over all pairs of atoms with $i < j$. The product of the multiple integrals is transformed using the substitution:

$$f(x) = \exp\left(-\frac{u_{ij}}{k\theta}\right). \tag{A.3}$$

The introduction of $f(x)$ allows

(A.4)
$$Z_{ex} = \frac{1}{V^N} \int_0^L dx_N \int_0^{x_N} dx_{N-1} \dots \int_0^{x_2} f(x_1) f(x_2 - x_1) \dots f(x_N - x_{N-1}) f(L - x_N) dx_N.$$

Now let us consider the sequence of functions

$$f_1(x) \equiv f(x),$$
$$f_m(x) = \int_0^x f(\xi) f_{m-1}(x - \xi) d\xi, \qquad m = 2, 3, \dots, \tag{A.5}$$

where f_m is obtained as convolution of the preceding function f_{m-1} with f. According to (A.4), we may write

$$Z_{ex} = \frac{1}{V^N} f_{N+1}(L). \tag{A.6}$$

Let us designate by $\phi(s)$ the Laplace transformation of the function $f(x)$:

$$\phi(s) = \int_0^\infty e^{-sx} f(x) dx, \qquad \mathrm{Re}(s) > 0, \tag{A.7}$$

so that the inverse is

$$f(x) = \frac{1}{2\pi i} \int_{c-i\infty}^{c+i\infty} e^{sx} \phi(s) ds, \tag{A.8}$$

where the positive number c is such that the path of integration lies to the right of all the poles of $\phi(s)$. By repeated application of the convolution theorem of the Laplace transformation, we obtain

$$\int_0^\infty e^{-sx} f_m(x) dx = (\phi(s))^m, \tag{A.9}$$

and because of (A.6) we may write

$$\int_0^\infty e^{-sL} \bar{Z}^{ex}(L) dL = (\phi(s))^{N+1}, \tag{A.10}$$

where $\bar{Z}_{ex} = Z_{ex} V^N$. Hence, by application of the Laplace transformation we obtain

$$\bar{Z}_{ex} = \frac{1}{2\pi i} \int_{c-i\infty}^{c+i\infty} e^{sL} (\phi(s))^{N+1} ds. \tag{A.11}$$

By proper selection of the integration contour (A.11) can be transformed into

$$\bar{Z}_{ex} = \frac{1}{2\pi i} \oint_c e^{sL} (\phi(s))^{N+1} ds. \tag{A.12}$$

If $l = L/(N+1)$ is the length per particle, we write

$$e^{sL} (\phi(s))^{N+1} = \left(e^{sl} \phi(s)\right)^{N+1} = e^{(N+1)\chi}, \tag{A.13}$$

where

$$\chi = sl + \ln \phi(s). \tag{A.14}$$

Hence for the saddle point s_0 we have the condition

$$\chi'(s_0) = l + \left[\frac{d}{ds}\ln\phi(s)\right] = 0, \tag{A.15}$$

so that in the vicinity of point s_0 there will be

$$\chi(s) = s_0 l + \ln\phi(s_0) + \frac{1}{2}\chi''(s_0)(s-s_0)^2 + \cdots. \tag{A.16}$$

Disregarding further terms of the expansion and placing (A.16) into (A.13) and (A.12), we obtain

$$\bar{Z}_{ex} = \left[e^{s_0 l}\phi(s_0)\right]^{N+1} \frac{1}{2\pi i}\oint_c e^{\left[\frac{1}{2}(N+1)\chi''(s_0)(s-s_0)^2\right]} ds. \tag{A.17}$$

On integrating along the chosen path which passes through point s_0, the integral in (A.17) gives the Poisson integral and, consequently, is of the order of $(N+1)^{1/2}$. For the asymptotic evaluation of $\bar{Z}^{ex}$, when $N \to \infty$, we use the logarithm of the factor which stands before the integral in (A.17). More precisely,

$$\lim_{N\to\infty} [\bar{Z}_{ex}]^{1/(N+1)} = e^{s_0 l}\phi(s_0). \tag{A.18}$$

Thus we obtain, asymptotically,

$$\bar{Z}_{ex} = e^{s_0 L}\left[\phi(s_0)\right]^{N+1} = e^{s_0(1+\epsilon)L_0}\left[\phi(s_0)\right]^{N+1}, \tag{A.19}$$

where L_0 is the reference length of the system, and ϵ is the strain. By placing (A.19) into (3.1) and taking into account the first equation in (4.3) and (2.1), we obtain for the stress

$$\begin{aligned}\sigma &= -\frac{k\theta}{V_0}\left(\frac{\partial \ln Z_{id}}{\partial\epsilon} + \frac{\partial \ln Z_{ex}}{\partial\epsilon} + \frac{\partial \ln Z_M}{\partial\epsilon}\right) = -\frac{k\theta}{V_0}\frac{\partial \ln Z^{ex}}{\partial\epsilon} \\ &= -\frac{k\theta}{V_0}\left(s_0 L_0 + (N+1)\left(l + \frac{d}{ds_0}\ln\phi(s_0)\right)\frac{\partial s_0}{\partial\epsilon}\right).\end{aligned} \tag{A.20}$$

When the condition in (A.13) is taken into consideration the stress becomes

$$\sigma = -\frac{k\theta}{V_0} s_0 L_0 = -\frac{k\theta}{A} s_0. \tag{A.21}$$

Thus it appears that $s_0 = -\sigma A/(k\theta)$. By placing this into (A.19), we obtain

$$Z_{ex} = \frac{1}{V^N} e^{-\frac{\sigma A L_0(1+\epsilon)}{k\theta}}\left[\phi(s_0)\right]^{N+1}, \tag{A.22}$$

where in accordance with (A.3) and (A.7)

$$\phi(s_0) = \int_0^\infty e^{-\frac{u_i(x)-\sigma A x}{k\theta}} dx. \tag{A.23}$$

REFERENCES

[1] J. J. Amalraj, *Effect of the Variable Material Properties on Purely Thermal Phase Transformation in Shape Memory Alloys Wire-Modeling and Experiments*, M.Sc. thesis, University of Alberta, Edmonton, AB, Canada, 1999.

[2] M. Baskes, *Modified embedded-atom potentials for cubic materials and impurities*, Phys. Rev. B, 46 (1992), pp. 2727–2742.

[3] E. Tadmor, M. Ortiz, and R. Phillips, *Quasicontinuum analysis of defects in solids*, Philos. Mag. A, 73 (1996), pp. 1529–1563.

[4] E. Tadmor, R. Phillips, and M. Ortiz, *Mixed atomistic and continuum models of deformation in solids*, Langmuir, 12 (1996), pp. 4529–4534.

[5] F. Abraham, J. Broughton, N. Bernstein, and E. Kaxiras, *Spanning the continuum to quantum length scales in a dynamic simulation of brittle fracture*, Europhys. Lett., 44 (1998), pp. 783–787.

[6] I. Fisher, *Statistical Theory of Fluids*, University of Chicago Press, Chicago, IL, 1964.

[7] G. Wagner, E. Karpov, and W. Liu, *Molecular dynamics boundary conditions for regular crystal lattices*, Comput. Methods Appl. Mech. Engrg., 193 (2004), pp. 1579–1601.

[8] K. Gall and M. Horstemeyer, *Atomistic simulations on the tensile debonding of an aluminum-silicon interface*, J. Mech. Phys. Solids, 48 (2000), pp. 2183–2212.

[9] F. Incropera and D. DeWitt, *Introduction to Heat Transfer*, John Wiley and Sons, New York, 1996.

[10] A. James and M. Lord, *Macmillan's Chemical and Physical Data*, Macmillan, London, UK, 1992.

[11] A. Jarvis, R. Hayes, and E. Carter, *Effects of oxidation on the nanoscale mechanisms of crack formation in aluminum*, ChemPhysChem, 2 (2001), pp. 55–59.

[12] G. Kaye and T. Laby, *Tables of Physical and Chemical Constants*, Longman, London, UK, 1993.

[13] S. Kim, *A Continuum Model for Phase Transitions in Thermoelastic Solids and Its Application to Shape Memory Alloys*, Ph.D. thesis, MIT, Cambridge, MA, 1995.

[14] W. Lai and B. Liu, *Lattice stability of some Ni-Ti alloy phases versus their chemical composition and disordering*, J. Phys.: Condens. Matter, 12 (2000), pp. L53–L60.

[15] L. Landau and E. Lifshitz, *Statistical Physics*, Oxford University Press, New York, 1990.

[16] D. Lide, *CRC Handbook of Chemistry and Physics*, 84th ed., CRC Press, Boca Raton, FL, 2003.

[17] M. Ortiz, A. Cuitino, J. Knap, and M. Koslowski, *Mixed atomistic continuum models of material behavior: The art of transcending atomistics and informing continua*, MRS Bull., 26 (2001), pp. 216–221.

[18] F. Mandl, *Statistical Physics*, John Wiley and Sons, New York, 1995.

[19] G. Wagner and W. Liu, *Coupling of atomistic and continuum simulations using a bridging scale decomposition*, J. Comput. Phys., 190 (2004), pp. 249–274.

[20] Q. Broughton, F. Abraham, N. Bernstein, and E. Kaxiras, *Concurrent coupling of length scales: Methodology and application*, Phys. Rev. B, 60 (1999), pp. 2391–2403.

[21] R. Hamilton, H. Sehitoglu, Y. Chumlyakov, and H. Maier, *Stress dependence of the hysteresis in single crystal NiTi alloys*, Acta Mater., 52 (2004), pp. 3383–3402.

[22] R. Miller, E. Tadmor, R. Phillips, and M. Ortiz, *Quasicontinuum simulation of fracture at the atomic scale*, Simul. Mater. Sci. Eng., 6 (1998), pp. 607–638.

[23] V. Stoilov and A. Bhattacharyya, *A theoretical framework of one-dimensional sharp phase fronts in shape memory alloys*, Acta Mater., 50 (2002), pp. 4939–4952.

[24] V. Stoilov, O. Iliev, and A. Bhattacharyya, *A moving boundary finite element method-based approach for the solution of one-dimensional problems in shape memory alloys*, Comput. Methods Appl. Mech. Engrg., 190 (2000), pp. 1741–1762.

[25] V. Shenoy, R. Miller, E. Tadmor, R. Phillips, and M. Ortiz, *Quasicontinuum models of interfacial structure and deformation*, Phys. Rev. Lett., 80 (1998), pp. 742–745.

[26] W. Liu, H. Park, D. Qian, E. Karpov, H. Kadowaki, and G. Wagner, *Bridging scale methods for nanomechanics and materials*, Comput. Methods Appl. Mech. Engrg., 195 (2006), pp. 1407–1421.